J Electroceram (2007) 19:67–79
DOI 10.1007/s10832-007-9048-z

The use of diffraction in the characterization of piezoelectric materials

Jacob L. Jones

Received: 15 September 2006 / Accepted: 19 December 2006 / Published online: 1 March 2007

Abstract X-ray and neutron diffraction have become powerful characterization tools in materials research. Their leading use in the characterization of piezoelectric ceramics includes the determination of structure, phase evolution, crystallographic texture, and lattice strain. The inherent electromechanical coupling of piezoelectric materials also allows the direct characterization of the converse piezoelectric effect. New advances in diffraction capabilities have recently enabled new problem solutions within this field. For example, the use of microdiffraction has the potential to characterize structural defects including cracks and domain walls. The development of time-resolved techniques has further opened doors to characterizing ferroelectrics in real-time under the application of cyclic electric fields. These recent advances as well as traditional uses of X-ray and neutron diffraction in the characterization of piezoelectric materials and the phenomenon of piezoelectricity are explored in this review. A focus is on characterization of bulk, polycrystalline ceramics, though novel approaches in thin films and single crystals are also reviewed. Challenges and future opportunities are discussed.

Keywords Diffraction · Piezoelectricity · Texture · Strain · X-ray scattering · Neutron scattering

1 Introduction

The diffraction of X-rays and neutrons from crystals has become invaluable to all areas of materials research. The use of diffraction as a characterization tool dates back nearly a century and the field continues to evolve today with new tools continually enabling new dimensions of characterization. The most traditional uses of diffraction lead to the characterization of crystal structure, phase evolution, particle size, crystallographic texture and lattice strains, and are undertaken throughout all fields of materials research. In piezoelectric materials, diffraction can also be applied to characterize the ferroelectric/ferroelastic domain structures [1] and, because of its electromechanical nature, the phenomenon of piezoelectricity itself. These two effects, illustrated schematically in Fig. 1, contribute to the electric-field-induced strain behavior of ferroelectric materials.

Today, wide varieties of diffraction instruments and characterization approaches are available. Selection of the proper source and instrument is a decision that should be based on required measurement time (largely limited by flux), peak shapes, widths and separation of peaks, sampling volume, instrument availability, and instrument location. The use of synchrotron X-ray sources can sometimes improve the quality of diffraction data through increases in both incident flux and resolution of the diffracted beam. Because neutrons can sometimes penetrate further into certain materials than X-rays, neutron diffraction can also improve the quality of data by increasing the sampling volume, and in certain cases increase the symmetry of the diffracted peak profiles. Because of their penetration depth, high-energy X-rays also enable greater sampling volume and less surface sensitivity than results obtained using laboratory X-ray sources. However, though national and international user facilities offer improved quality of the diffraction data and excellent user support expertise, these facilities are sometimes over-subscribed and access is limited. Therefore, the availability of quality laboratory diffraction equipment is also highly valuable in the characterization of piezoelectric materials.

J. L. Jones (✉)
Materials Science and Engineering, University of Florida, Gainesville, FL, USA
e-mail: jjones@mse.ufl.edu

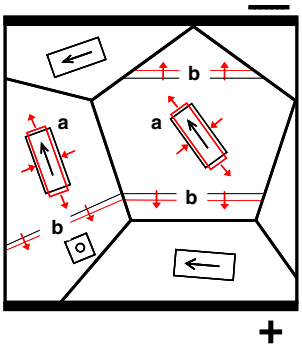

Fig. 1 Schematic of the intrinsic piezoelectric strain (**a**), and domain switching or domain wall motion (**b**), in response to an applied electric field in a ferroelectric polycrystalline ceramic with tetragonal symmetry. *Arrows* indicate directions of strain and domain wall movement during the electric field application

This paper offers a review of the use of X-ray and neutron diffraction in the characterization of piezoelectric materials, including both traditional uses and recent progress made in this field. The discussion focuses on polycrystalline materials, as an entirely independent review could be offered for diffraction from single crystals, particularly considering the wealth of recent investigations into the structure of relaxor single crystals. Nevertheless, single crystal diffraction is discussed where appropriate. The remaining sections of this paper subdivide the discussion into topical areas. These include:

2. Structure determination,
3. Phase evolution,
4. Crystallographic texture,
5. Domain switching,
6. Lattice strains,
7. Diffuse scattering and extinction effects,
8. Microdiffraction, and
9. Time-resolved techniques.

Future opportunities which span these areas are further discussed in an additional concluding section at the end.

2 Structure determination

Characterization using diffraction patterns can be accomplished either by evaluating the characteristics of single diffracted peaks (e.g., position, profile shape, intensity) or through the simultaneous consideration of multiple diffracted peaks. The latter is most beneficial for structure determination because inherently more crystallographic information is contained within multiple diffracted peaks. For example, consider the extraction of lattice parameters from a powder diffraction pattern, where errors from sample positioning in the Bragg plane influence lattice parameters calculated from single peaks. This error is substantially reduced by extrapolating multiple lattice parameter measurements to $(\theta)=90$ [2]. Another demonstration of the benefit of using the information contained in multiple peaks in piezoelectric materials is found in morphotropic phase boundary (MPB) ceramics, where domain wall microstrains and secondary phases are difficult to distinguish from lower symmetry phases [3].

To make use of all of the information contained within a diffraction pattern, one can use a whole powder pattern fitting routine, the most prevalent approach being the Rietveld method [4]. Rietveld refinement guidelines and guidelines for the publication of results can be found in McCuster et al. [5] and Young et al. [6], respectively. Within the Rietveld method, the crystal structure, instrument geometry and optics, lattice parameters, phase fractions, crystallographic texture, and microstrains can be modeled [7]. The entire diffraction pattern is then constructed from this model because most of the underlying physics contributing to a diffraction pattern is known. A least squares refinement is then carried out on all modeled parameters until a best fit is found between the measured and calculated diffraction patterns. Crystallographic and microstructural parameters can therefore be extracted via the Rietveld method as a function of material processing history, starting powder compositions, and applied loads such as hydrostatic pressure or electric field. The crystallographic parameters of most interest here are the lattice parameters, atomic occupancies and atomic positions, the last of which enables calculation of other characteristics such as bond lengths and octahedral tilting.

Strictly speaking, the Rietveld method is a technique for refining structures because it first requires a good approximation of the starting parameters. Thus it is not a general method for structure determination, particularly for the determination of unknown structures [8]. Nonetheless, the Rietveld method has proven successful in extracting crystal structure information in piezoelectric lead zirconate titanate (PZT) [3, 9–11], solid solutions of lead zinc niobate—lead titanate (PZN-PT) and lead magnesium niobate—lead titanate (PMN-PT) [12–16], barium zinc tantalate (BZT) [17], potassium niobate ($KNbO_3$) [18] and bismuth titanate (e.g., $Bi_4Ti_3O_{12}$) [19, 20] compositions.

Though the Rietveld method concerns the refinement of all parameters (including structure) leading to the diffraction pattern, alternative approaches are available, such as that introduced by Le Bail et al. [21], where individual integrated intensities are extracted free of structural constraints. That is, instead of refining the structure from the measured profiles, only the intensities themselves and the profile shape function are refined. Sani et al. recently used this approach to determine the structure of PZT located near the MPB as a function of hydrostatic pressure [22].

In some piezoelectric materials, a spontaneous polarization arises through the separation of the positive and negative charge centers. The spontaneous polarization (P_s) can be estimated from the results of a refined structure because the average atomic positions are determined

through such a method. The calculated spontaneous polarization (P_s) can be approximated by:

$$P_s = \sum_i (m_i \times \Delta x_i \times Q_i e)/V \quad (1)$$

where for the ith atom, m_i is the multiplicity, Δx_i is the atomic displacement from the neutral position along the polarization axis, $Q_i e$ is the ionic charge, and V is the unit cell volume (e.g., see [23]). When the spontaneous polarization is to be calculated from the determined structure, neutron diffraction is valuable because the larger scattering factors of lighter elements such as oxygen enable better accuracies of their position. Though the resolution is more often better when using data obtained from X-ray diffraction, the errors in oxygen positions can result in large errors in P_s. A refinement which combines both X-ray and neutron diffraction profiles to determine a structure can take advantage of the benefits of both techniques [24].

Calculations of P_s for piezoelectric materials are frequently encountered in the literature, and should be interpreted cautiously. These calculations neglect electronic polarization and defects, assume ionic bonding, and rarely account for the errors associated with the atomic positions. Therefore, a single P_s value obtained from a single refinement is of little value. However, works demonstrating *changes* in the calculated crystal structure parameters as functions of applied loading or processing parameters provide more reliable information. This is because trends in ΔP_s are more reliable than the absolute P_s values if one assumes the error contributions are somewhat consistent. For example, Forrester et al. have recently measured the change in spontaneous polarization of PZN single crystals from 4.2 K (tetragonal, 35 $\mu C/cm^2$) to 384 K (cubic) [12] and show a clear trend in P_s with temperature.

Good quality structure refinements are best performed on randomly-oriented powder samples to eliminate errors in modeling of crystallographic texture and other anisotropic effects. However, when a refinement necessarily proceed using diffraction data obtained from a sintered polycrystalline material, it is best if the polycrystalline material is randomly-oriented. In other words, the randomly-oriented bulk sample can be rotated and a second refinement using data from a different scattering angle will generate the same structure results as in the first refinement. This is valuable for studying crystal structures in the absence of loading or under hydrostatic conditions; most recent refinements have therefore characterized changes in structure as a function of temperature or hydrostatic pressure. However, this approach presumes that the average internal stresses of each grain in the polycrystal are hydrostatic, which may not be the case in highly anisotropic materials. Furthermore, this isotropic assumption limits the ability of this approach to accurately determine structure in textured microstructures and structure changes as a function of deviatoric loading. This is unfortunate in piezoelectric materials because 'uniaxial' driving electric fields are first-rank tensors which generate anisotropic electromechanical strains and atomic displacements. Even in the absence of applied electromechanical loading, textured microstructures may exhibit a directional dependence of the structure (e.g., atomic positions may be different in differently-oriented grains). Thus, the development of tools for anisotropic crystal structure refinement, particularly during in situ electromechanical loading, would enable much-needed research in this field. Such an approach may be able to distinguish the orientational dependence of electric-field-induced changes in spontaneous polarization. Analogous methods have already been developed for the study of anisotropic crystallographic microstrains using Rietveld refinement [25, 26].

Further advances in structure determination will most likely include the use of additional information available in the diffraction pattern, such as through the extraction of the pair distribution function (PDF) [27, 28]. PDF studies give information on short-range ordering and are not limited to bulk-average order measured directly in diffraction. This technique therefore has the ability to answer questions in the periodicity of cation ordering [29], nano-domain boundaries [30–32], and antiferroelectric ordering [33]. Some early work in this area has already been reported in morphotropic phase boundary materials [34, 35].

3 Phase evolution

Phase identification is particularly important in piezoelectric materials because the most advantageous properties are often found at compositions near MPBs, where multiple phases may coexist and can sometimes only be distinguished using higher-resolution instruments. A low degree of crystallographic distortion in the ferroelectric phase can sometimes also lead to the false conclusion of a higher-symmetry phase. Fig. 2 illustrates two different peak profiles obtained for the bismuth titanate composition $Na_{0.5}Bi_{4.5}Ti_4O_{15}$, one using a laboratory diffractometer with a Cu tube source and the second using a synchrotron X-ray source coupled with a crystal analyzer detector. $Na_{0.5}Bi_{4.5}Ti_4O_{15}$ has a crystallographic lattice aspect ratio (a/b) of 1.005 [19], which cannot be resolved using the lower-resolution laboratory diffractometer. For distinguishing small crystallographic distortions or phases of low-symmetry materials where peaks may be highly overlapped, phase identification can be aided by the use of the Rietveld method [36, 37].

In piezoelectric materials, phase evolution is of interest during and after processing as well as during and after application of stress or electric fields. In particular, MPB

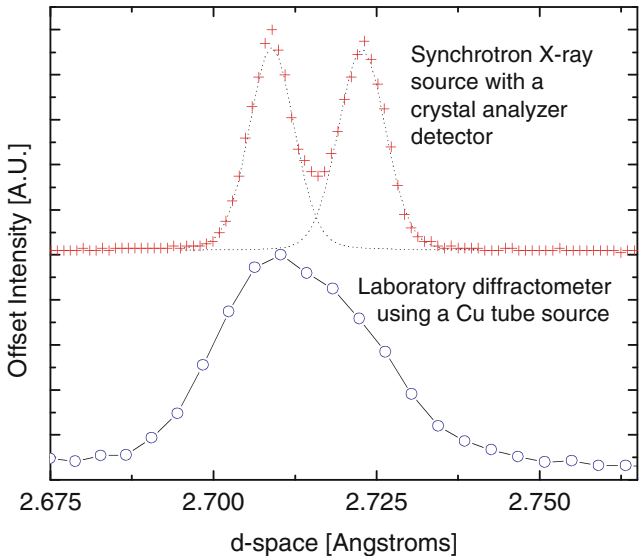

Fig. 2 Two diffraction peaks from a polycrystalline $Na_{0.5}Bi_{4.5}Ti_4O_{15}$ ceramic obtained using two different instruments. The *upper pattern* was obtained using a synchrotron X-ray source at the National Synchrotron Light Source, beamline X18A, with a Ge (111) crystal analyzer detector. The *lower pattern* was obtained using a Siemens D500 diffractometer with an energy-dispersive detector, set to analyze a window of 460 eV. The upper pattern contains two pseudo-Voigt peak shape functions centered at the orthorhombic (200) and (020) lattice plane positions

compositions can exhibit field-induced phase changes during electrical or mechanical loading. Such a phenomenon can also be described as 'phase switching' [38] or interphase boundary motion [39].

Most notably, studies of phases near the MPB in PZT have dramatically influenced this field in recent years. Using high-resolution synchrotron diffraction, Noheda et al. first demonstrated a monoclinic 'phase' in PZT ceramics near the MPB at low temperatures [40]. This phase was also found to exist at room temperature after electrical poling [41]. More recent efforts by Viehland et al. have suggested that this apparent monoclinic phase is comprised of unique tetragonal and rhombohedral microdomains, or an 'adaptive phase,' which appears to be monoclinic when using macroscopic diffraction approaches [30–32]. A review on these competing themes is given by Noheda et al. [42] and more recently within this volume by Davis [43]. Even without considering the possibility of monoclinic symmetry, however, tetragonal and rhombohedral phases have been known to coexist near MPB regions. For example, tetragonal and rhombohedral phases have been observed within the same grain of a ceramic PZT near the MPB by Hoffmann et al. [44]. Similarly, Rogan et al. demonstrated that a $PbZr_{0.49}Ti_{0.51}O_3$ ceramic contained roughly 79% of the tetragonal phase and 21% of the rhombohedral phase by using the Rietveld method to refine the fraction of tetragonal and rhombohedral phases [45].

Another impressive example of the study of phase evolution in piezoelectric materials is provided by Misture [46], where an in situ laboratory X-ray system has enabled the study of reaction mechanisms. Fig. 3 shows the changes in the diffraction pattern as a function of time and temperature during the production of the Aurivillius-oxide $Bi_4Ti_3O_{12}$. The Rietveld method was used to quantify the phase fractions as a function of time and a rate constant is extracted for each temperature, enabling the reaction kinetics of $Bi_4Ti_3O_{12}$ growth to be determined.

4 Crystallographic texture

When the probability of any given crystallographic orientation is non-random, the material is referred to as being 'textured' [47]. Diffraction has long been integral to measurement of texture in polycrystalline materials. In piezoelectric materials, the purpose of crystallographic texture is to generate anisotropic properties in the polycrystalline ceramic, typically leading to an enhanced piezoelectric response in a preferred direction relative to the same property in a randomly oriented ceramic. This is primarily accomplished through a preferential alignment of the crystallite P_s vectors. Crystallographically textured ceramics thereby offer a compromise between high-priced single crystal materials and randomly-oriented polycrystalline ceramics. Some bulk ceramics that have recently been investigated for the influence of grain texture include Aurivillius oxides [48–54], tungsten bronze structured (Sr,Ba)Nb_2O_6 [55, 56], PMN-PT [57–59], and $Na_{1/2}Bi_{1/2}TiO_3$-$BaTiO_3$ [60, 61]. Some of these are reviewed by Messing et al. [62].

In bulk piezoelectric materials, texture can be induced to the grain orientations through forming processes such as hot forging, tape casting, and uniaxial pressing, or to the

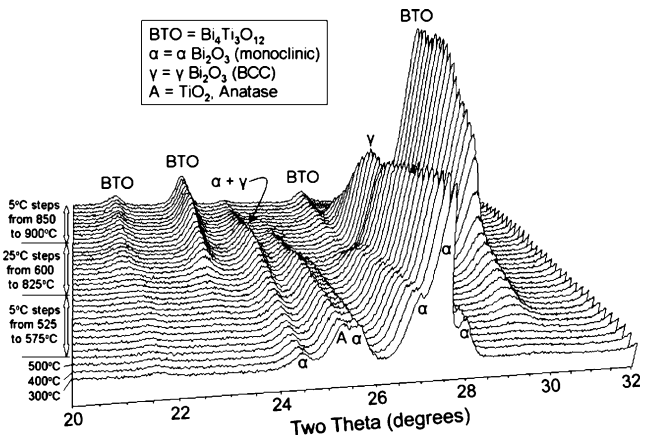

Fig. 3 X-ray diffraction patterns as a function of temperature during the formation of $Bi_4Ti_3O_{12}$. Patterns obtained in situ using a laboratory X-ray source and a linear PSD (from Misture [46])

ferroelastic/ferroelectric domain structure through the poling process. Both of these can be considered as types of texture because certain crystallographic orientations become non-random in both cases. In the case of ferroelastic/ferroelectric texture, preferred orientation is induced to the sub-grain (domain) structure. In both cases, the texture leads to characteristic changes in the intensity of certain peaks in the diffraction pattern. We have previously referred to these two different types of texture as 'grain texture' and 'domain texture' [48]. Pole figures describing the degree of orientation induced to the grains and domains of a tape-cast $Na_{0.5}Bi_{4.5}Ti_4O_{15}$ ceramic are shown in Fig. 4. While an initial preferred orientation exists prior to electrical poling, the process of electrical poling induces a greater degree of preferred orientation of the 200 pole (ferroelastic long axis). This section discusses recent efforts to quantify grain texture in piezoelectric materials; domain texture is discussed in detail in the following section.

Many diffraction methods have been used for measuring texture in piezoelectric ceramics. Qualitative assessments of the degree of orientation have been made using the Lotgering factor [63], which is a calculation of a relative intensity ratio of certain peaks in the diffraction pattern of the textured material compared to the same calculation in a randomly oriented material. However, the calculated 'degree of orientation' is only qualitative and dependent upon the type and number of reflections used in the calculation [19]. This is not surprising given that even Lotgering referred to this as a semi-quantitative "estimate" of the degree of orientation [63]. Of course if applied consistently, it does offer a quick method for comparing the degree of orientation in a series of samples using a laboratory diffractometer. However, it should not be considered as a quantitative measure.

Better quantitative measures of texture are made through measurement of complete pole figures. In some instances, the pole figure $P_{hkl}(\alpha,\beta)$ can be modeled using the March-Dollase equation [64, 65], which assumes a fiber-type texture (constant with azimuthal angle β) consisting of a textured material fraction, f, and a parameter r which defines the strength of the texture. Thus, the pole figure is modeled by the equation:

$$P_{hkl}(f,r,\alpha) = f\left(r^2\cos^2\alpha + \frac{\sin^2\alpha}{r}\right)^{-3/2} + (1-f). \quad (2)$$

For describing texture in PMN-PT ceramics prepared by templated grain growth (TGG), Brosnan et al. have recently compared the above measurement approaches to electron backscattered diffraction and determined that fitting Eq. 2 to measured rocking curves was the most time-efficient and comprehensive of these techniques for quantifying texture [59].

Still better quantitative assessments of texture can be made through a calculation of the orientation distribution function (ODF), in which the pole density value $f(g)$ represents the multiple of a random distribution (mrd) and the orientation g is defined by the three Euler angles ϕ_1, Φ, and ϕ_2. The ODF can be represented directly or through an expansion of spherical harmonics. Reference texts on texture analysis using the ODF can be found in [47, 66, 67]. The ODF is typically calculated using pole-figure inversion or full-pattern Rietveld refinement for texture. In the former case, the measured pole figures are used to reconstruct the ODF. In full-pattern Rietveld refinement for texture, intensity changes due to texture are extracted from the diffracted intensity refinement (Section 2) and used in calculation of the ODF [36, 37]. Time-of-flight (TOF) neutron diffraction often necessitates such an approach [37, 68]. The use of the ODF in describing grain textures in piezoelectric materials has been demonstrated in both bulk ceramics [19, 69] and thin films [70–72].

Mechanistically, the influence of texture on piezoelectric properties is not fully understood. Recent experimental investigations have suggested that both a percolation of spontaneous polarization [55] and the alignment of ferro-

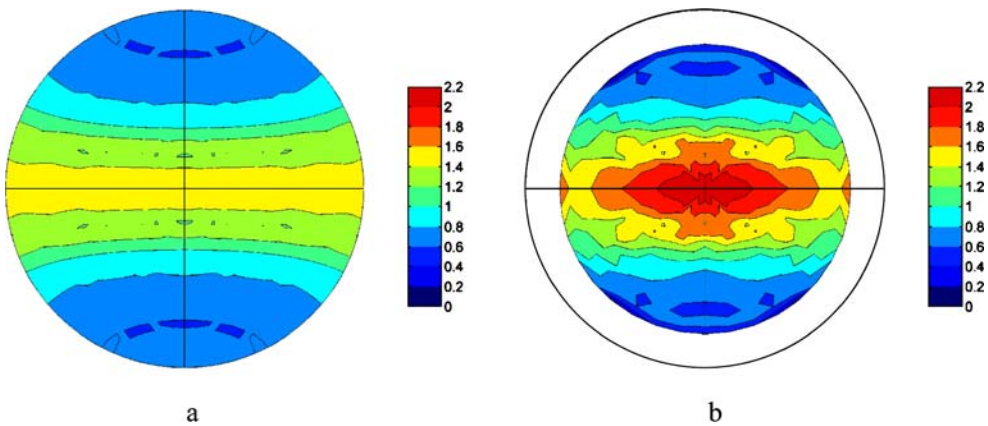

Fig. 4 200 pole figures representing the texture of the ferroelastic long axis in a tape-cast $Na_{0.5}Bi_{4.5}Ti_4O_{15}$ ceramic before electrical poling (**a**) and after electrical poling (**b**). Degree of preferred orientation given in the unit multiple of a random distribution (mrd) and presented on an equal area projection. The measured region is smaller in (**b**) because the measurement was performed in reflection geometry using discrete intensity measurements (after Jones et al. [48])

elastic distortion directions [52] can influence the electromechanical properties. While it has been argued that the percolation mechanism proposed by Duran et al. [55] is a result of the semi-quantitative texture analysis approach employed within that work [19], a more complete understanding of the microstructural interactions should be pursued. To this end, the influence of texture on piezoelectric properties would be aided by more rigorous constitutive models of texture in electromechanical materials. Such models should account for the interaction of the crystallite piezoelectric tensors of neighboring orientations or the effective medium boundary condition. In order to correlate experimental results with the model, these models must also properly describe preferred orientation. Though a few recent works by Garcia et al. [73] and Ruglovsky et al. [74] have begun to incorporate grain–grain and grain-bulk interactions in textured piezoelectrics, more work is needed, particularly in coupled theoretical/experimental studies, the examination of various crystal classes and grain shape distributions, and the modeling of extrinsic effects, such as domain wall contributions, to electromechanical properties.

The future of quantitative texture analysis may involve the incorporation of the additional dimensionalities of spatiality, lattice defects and residual stress into a complete microstructure distribution function, $G(x)$ [75]. Thus, micron-size-scale diffraction techniques for measuring the spatial distribution of grain and domain orientations will become necessary in the near future. To this end, some recent advances in microdiffraction are discussed in Section 8.

5 Domain switching

As discussed in the previous section, domain switching induces a form of crystallographic texture. This texture is expressed in diffraction patterns as an interchange in intensity between crystallographically degenerate peaks. The use of diffraction in the characterization of domain switching is not exclusive to piezoelectric materials. Other oxide materials exhibit this phenomenon including zirconia-containing ceramics [76–78] and lanthanum oxide ceramics [79–81]. Domain switching of 90° domains in perovskite tetragonal ceramics is demonstrated through an intensity interchange between the 002 and 200 peaks. The change in intensity of these peaks as a function of angle from the electric field in a tetragonal PZT material is shown in Fig. 5. Parallel to the electric field, the intensity of the 002 peak is strongest. With increasing angle to the electric field direction, the intensity of the 002 peak decreases.

In prior work, it has been demonstrated that the degree of domain switching in an initially randomly-oriented polycrystalline ceramic is a function of crystallographic symmetry [82]. The possible degree of switching increases with the number of ferroelastic variants. Similarly, the domain switching *distributions*, or the degree of domain switching as a function of angle from the loading axis, are also a function of crystallographic symmetry. The calculated saturation distributions are shown in Fig. 6a and b for three unique ferroelastic crystal symmetries loaded in tension and compression, respectively.

The distributions of domain orientations achieved in real ceramics can be measured directly at all orientations or interpolated through a few discrete measurements. The domain textures illustrated in Fig. 4b result from direct measurements in several sample orientations. For analytical descriptions, domain distributions have been approximated using the March–Dollase function (Eq. 2) [45, 83] as well as a $\cos^2\alpha$ function, where α represents the angle from the electric field or uniaxial stress axis [84]. Alternatively, the degrees of domain switching achieved in real ceramics can be measured using techniques such as those discussed in Section 4. For example, Jones et al. reported the degree of ferroelastic switching achieved in tetragonal PZT ceramics as a function of stress using Rietveld refinement for texture from TOF neutron diffraction patterns. A comparison of these distributions to the saturated distribution is shown in Fig. 6c. The degree of ferroelastic switching increases with applied compressive stress and approaches but does not reach the maximum possible saturation switching state.

Because non-180° domain switching results in an interchange in intensity of certain peaks, the degree of

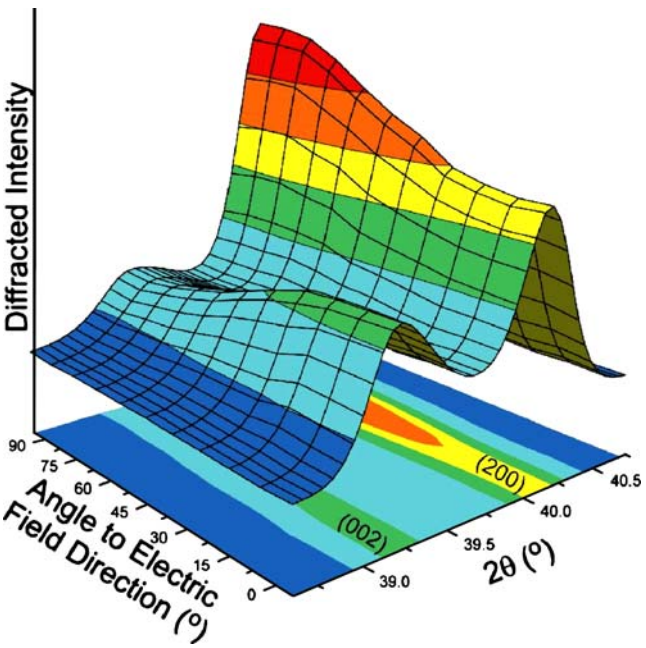

Fig. 5 Diffraction profiles of the (200) and (002) reflections in a tetragonal PZT ceramic as a function of angle from the poling axis. The intensity changes represent the degree of ferroelastic domain switching attributed to the electrical poling process. Data obtained using neutron diffraction at the Australian Nuclear Science and Technology Organisation (ANSTO)

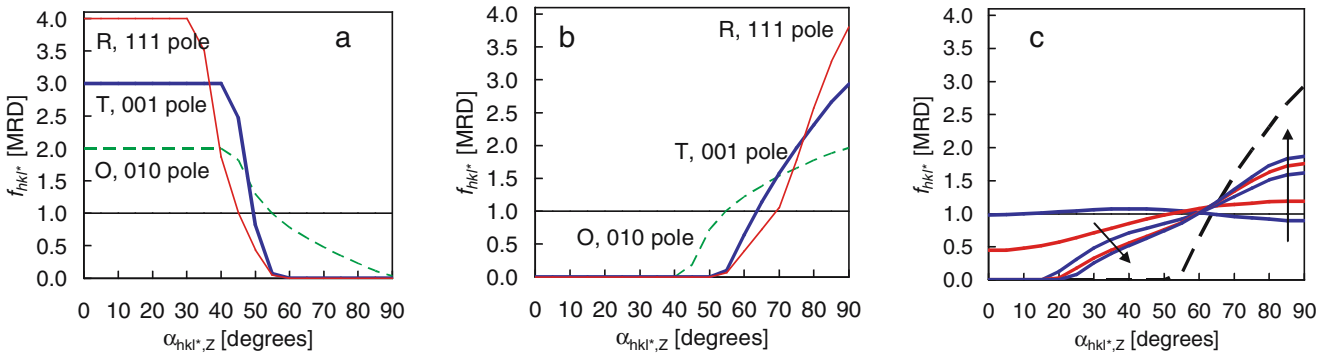

Fig. 6 Distribution functions of saturated ferroelastic switching in tension (**a**) and compression (**b**) of initially randomly oriented ceramics of rhombohedral (*R*), tetragonal (*T*), and orthorhombic (*O*) symmetry in the unit multiple of a random distribution (*MRD*) (after Jones et al. [82]). In (**c**), the degree of ferroelastic switching in soft, tetragonal PZT ceramics as a function of increasing stress (10, 50, 100, 150, and 200 MPa) is compared to the saturated distribution (– –) (after Jones et al. [91])

domain switching can also be calculated directly from the change in relative intensities. These formulations are described and the two approaches, that of direct measurement in certain orientations versus interpolation using the ODF, are compared in Jones et al. [85]. Many other works have used this or similar peak intensity comparisons to quantify the degree of ferroelastic switching in a particular sample direction [9, 44, 45, 52, 81, 83–89]. Typically, these measurements require a value for the integrated intensity of each diffracted peak. Daniels et al. have recently demonstrated that the split Pearson VII-type function best describes the tetragonal 002 and 200 peaks [90].

One of the advantages of describing complete distributions of domain switching as opposed to single measurements in a given sample direction is that complete distributions of switching can be used in subsequent quantitative calculations. This is because single crystal properties are related to the polycrystalline properties through the ODF. For example, Jones et al. use the distributions in Fig. 6c, combined with the crystallographic lattice aspect ratio *c*/*a*, to calculate the contribution of ferroelastic switching to the bulk macroscopic strain [91]. They find that ferroelastic switching contributes approximately 70% to the remanent macroscopic strain measured after unloading from 200 MPa. Remanent lattice strains are inferred to comprise the remaining ~30%, correlating with the remanent lattice strain measured from the 111 peak shift. This relationship has also been applied to extract the contribution of ferroelastic domain switching to the strain measured during cyclic electrical loading (the converse piezoelectric effect) [92]. It was determined that ~34% of the macroscopic strain attained during application of a subcoercive unipolar driving electric field resulted from ferroelastic domain switching.

It would be worthwhile in future work to continue exploring these relationships in more detail. Initial relationships have started to develop, as previously mentioned for the case of relating the single crystal strain (*c*/*a*) to the bulk macroscopic strain under mechanical and electrical loading. In piezoelectric materials, it would be interesting to relate the single crystal polarization to polycrystalline polarization through the ODF. With the recent demonstration of the ability to measure polarization inversion or 180° domain switching by Grigoriev et al. [93], the single crystal polarization calculated in a Rietveld refinement (Eq. 1) can be coupled with the ferroelectric/ferroelastic domain orientation distribution, resulting in a direct calculation of the 'absolute' polarization in a polycrystalline aggregate. Other properties which could also be explored through such quantitative approaches are dielectric permittivity [94], thermal conductivity and expansion [95], ionic and electrical conductivity [96], and other coupled properties in multiferroic systems [97]. Some of these properties are also influenced by other microstructural effects such as grain boundaries and grain misorientations. Nonetheless, a first approximation is necessary. Whereas the relationships between domain distributions and macroscopic properties have only thus far been developed for initially randomly-oriented materials, the most complete approach would incorporate both grain and domain texture and grain–grain and domain–domain interactions. This more complete microstructure description would enable integration of texture measurements and anisotropic properties across a wide range of bulk ceramics and thin films.

6 Lattice strains

Crystallographic lattice strains are measured in diffraction as shifts in the diffraction peak position (uniform lattice strains) or as peak broadening (non-uniform lattice strains) [98]. Therefore, the intrinsic component to the electric-field-induced piezoelectric strain (converse piezoelectric effect) can be measured directly using diffraction.

Under electrical loading, a number of researchers have found that the maximum uniform lattice strain was

observed in grains oriented with the 111_{pc} or 001_{pc} crystallographic direction parallel to the electric field for tetragonal and rhombohedral PZT ceramics, respectively, [41, 44, 99–101]. In other words, the maximum piezoelectric strain is not observed along the spontaneous polarization direction in either composition. While the results of the rhombohedral composition are consistent with theoretical calculations, the results for tetragonal contradict those of theory [39, 102–105]. For tetragonal ceramics, theory predicts the maximum piezoelectric strain parallel to the 001 direction. The recent results of Budimir et al. [103], however, demonstrate that the direction of maximum piezoelectric response can be changed by applied compressive stress. With increasing compressive stress along the 001 direction, the maximum piezoelectric response in tetragonal PZT ceramics is redirected towards the 111 direction. Therefore, the inconsistency between the lattice strains measured in diffraction and the models may be contributed by crystallites which are influenced by other factors such as the stress induced from the surrounding domains and grains. These directionally dependent stresses can be measured using diffraction.

From a microstructural perspective, stress may be developed within the grains during cooling from high-temperature processing or during electrical poling. During electrical poling, for example, a positive longitudinal sample strain is induced as a result of the increasing volume fraction of the c-oriented domain at the expense of the *a*- and *b*-oriented domains. This longitudinal domain switching strain is best understood by considering a grain oriented such that its crystal axes are coincident with the sample axes. The strain contributed by the increasing volume fraction of the *c*-oriented domain within this grain is not fully realized macroscopically because of misoriented neighboring grains which resist this larger degree of longitudinal strain [82]. Therefore, there may be compressive strains on each *c*-domain parallel to the electric field. Further evidence for a compressive stress lies in the fact that electrical poling does not lead to saturation of domain switching [85]. Internal stresses may therefore control the attainable degree of switching and also the piezoelectric response in polycrystalline ceramics. Recent fracture toughness measurements have also suggested that the internal stresses induced when cooling a ferroelastic material through its Curie temperature are a function of the number of ferroelastic variants [106]. Materials with fewer ferroelastic variants may exhibit higher degrees of intergranular stress. Incidentally, both crystal symmetry and strain can be measured using diffraction.

Recently, Hall et al. [101] have suggested that the 111 lattice strain in tetragonal PZT is due to intergranular strain developed during poling. They find the lattice strain exhibits a $\cos^2\alpha$ dependence, where α is the angle to the electric field. Therefore, the 111 lattice strain is tensile parallel to the poling direction and compressive perpendicular to the poling direction. Hall et al. have also reported similar angular dependencies for rhombohedral PZT [84], in agreement with the work of Shirakihara et al. [107]. Unfortunately, measurement of the stress in the 111 direction does not describe the longitudinal stress applied to the *c*-oriented tetragonal domain. More diffraction measurements are necessary to characterize this effect. In accordance with the directional dependence of the induced stress state mentioned above, the stresses of all crystallographic directions should be evaluated. Of particular importance with regard to the internal stresses is the measurement of the 002 and 200 strains which may control the piezoelectric response in tetragonal PZT [103].

Under compressive mechanical loading, Rogan et al. [45] reported the strain in the 001 and 100 directions of tetragonal PZT ceramics and in the 111_{pc} and $1\bar{1}0_{pc}$ directions of the rhombohedral phase. In contrast to the results from electrical loading, they find that the greatest strain is along the polar direction (ferroelastic long axis) in both crystal systems. Jones et al. [108] measured the lattice strains of the 002, 200, and 111 peaks as a function of angle from the compressive axis in tetragonal PZT ceramics and again found that the 002 lattice strains are larger than the 200 and 111, confirming the results of Rogan et al.

Using high-energy synchrotron X-ray diffraction and collecting complete Debye–Scherrer rings, Vullum et al. have recently characterized strains in other ferroelastic materials, namely $LaCoO_3$-based materials [81]. Their experimental approach, utilizing a two-dimensional detector, permits simultaneous collection of multiple reflections in multiple sample directions, a powerful approach for studying the micromechanics of ferroelastic systems. Various single crystal models have predicted the piezoelectric response when the electric field is applied in different crystallographic directions and under compressive pre-stress (e.g., [103]). An instrumental arrangement similar to that employed by Vullum et al. would facilitate the measurement of such complex, orientation-dependent crystallographic strains in polycrystalline materials. Using such an arrangement, one can simultaneously measure the experimental lattice strain of multiple crystallographic directions in multiple sample directions. A multi-peak strain and texture assessment could also be used to calculate the intrinsic contribution to the macroscopic strain using strain-averaging techniques developed by Daymond et al. [109, 110].

7 Diffuse scattering and extinction effects

The intensity of Bragg reflections and the diffuse scattering near Bragg peaks enables characterization of microstructural

features such as domain walls and polar nano-regions (PNRs). In simple terms, diffuse scattering is the redistribution of diffracted intensity from Bragg peaks due to short-range spatial and/or temporal deviations of the local structure from that of the average bulk. This appears either as a uniform background contribution or as changes in the peak profile shape. The diffuse scattering associated with the peak asymmetry in a tetragonal PZT ceramic is shown in Fig. 7. In contrast, extinction leads to a decrease in the total Bragg scattering intensity from that expected by calculation using a crystal mosaic structure. The degree of extinction depends upon the perfection of the crystal and the scattering power of the planes in question. Measurements of both effects can be used in the characterization of piezoelectric materials.

The influence of domain wall strains on diffuse scattering has been studied in polycrystalline ceramics by Ustinov et al. [111], Hayward and Salje [112], and Boysen [113]. Ustinov et al. modeled the influence of $\{110\}_{pc}$ domain walls in tetragonal perovskite ceramics and found that the diffuse scattering between the tetragonal 002 and 200 peaks is a function of domain wall thickness and density [111]. In more recent work, Daniels et al. have estimated the density of domain walls in tetragonal PZT ceramics by attributing the deviation from peak symmetry to the diffuse scattering and subsequently the domain-wall, strain-affected volume [90]. Glazer et al. have also used diffuse scattering in electron diffraction patterns to elicit short range order in PZT compositions near the MPB [114]. Similar diffuse scattering measurements across the MPB by X-ray and neutron diffraction would confirm the global behavior in the bulk of the material.

In single crystals, Stock et al. [115] and Xu et al. [116] used diffuse scattering to study the short-range ordering of PNRs in relaxor ferroelectric PMN-60 PT and PZN. PMN-60 PT exhibited little diffuse scattering, indicating long-range order or the absence of significant PNRs [115]. PZN, on the other hand, exhibited PNRs with real-space shape anisotropy, evidenced by a field-induced change to anisotropic diffuse scattering [116].

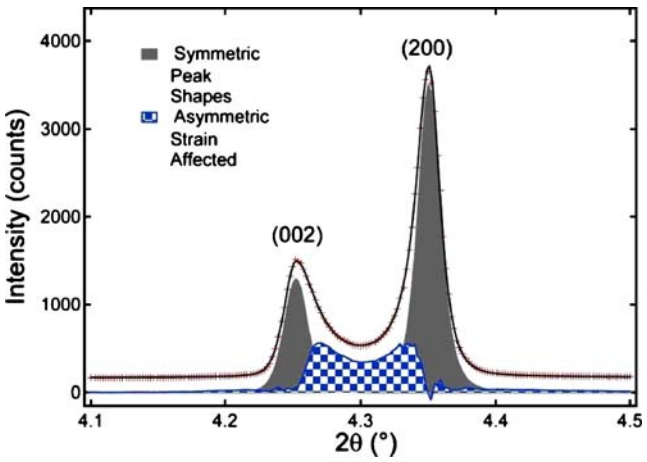

Fig. 7 Deviation from symmetric peak shape functions in a tetragonal PZT ceramic attributed to domain wall strain-affected volume. Data obtained from high-energy synchrotron diffraction in transmission geometry (after Daniels et al. [90])

Opportunities exist in this area for systematic investigations of diffuse scattering as a function of composition through MPBs of various material systems. Furthermore, correlations could be developed between diffuse scattering profiles and domain structure models, particularly as a function of temperature and electric field. The use of extinction conditions has also not been as widely applied, but exhibits the potential for the study of 180° domain walls during electrical loading and migration of other point, line, or planar defects in large-grain-size or single crystal piezoelectric materials.

8 Microdiffraction

With the increasing flux available at synchrotron X-ray sources, efficient diffraction using an incident beam size on the micron-size scale is possible, thus permitting the spatial characterization of piezoelectric materials. The opportunities in microdiffraction include the study of both sample inhomogeneity and the characterization of local defects such as cracks and domain walls.

In a noteworthy example, Rogan et al. recently measured the microstrains at a 90° domain wall boundary in single crystal $BaTiO_3$ using a 1×1 μm^2 beam size at the Advanced Light Source (ALS) [117]. They found that the strains at a 90° domain wall exceed $1.5\cdot10^{-3}$. Using an even smaller 800 nm beam size at the Advanced Photon Source (APS), Do et al. have observed polarization fatigue spatially with respect to the electrode edges in a tetragonal PZT thin film [118]. On a larger size scale, Jones et al. have recently used a 50×50 μm^2 beam size to map ferroelastic switching around a crack tip in a loaded compact tension specimen [Jones and Üstündag, unpublished work]. A map of the domain switching and lattice strains under loading at a stress intensity factor just below the initiation toughness is shown in Fig. 8. The degree of domain switching near the crack tip is 1.1 mrd, the maximum 111 lattice strains are approximately $2.0\cdot10^{-4}$, and the spatial distributions are on the order of 1 mm.

Recent microdiffraction work in non-piezoelectric materials has demonstrated the feasibility of measuring single grain orientations embedded within a polycrystalline material and even the characterization of sub-grain features such as dislocations [119]. Combined with high-energy X-rays, fast or real-time measurements are also possible, enabling "X-ray microscopy in four dimensions" (e.g., see Juul Jensen et al. [120]). Such a technique may prove valuable in characterizing the dynamics of domains and cracks to applied cyclic electromechanical loads. Certainly the

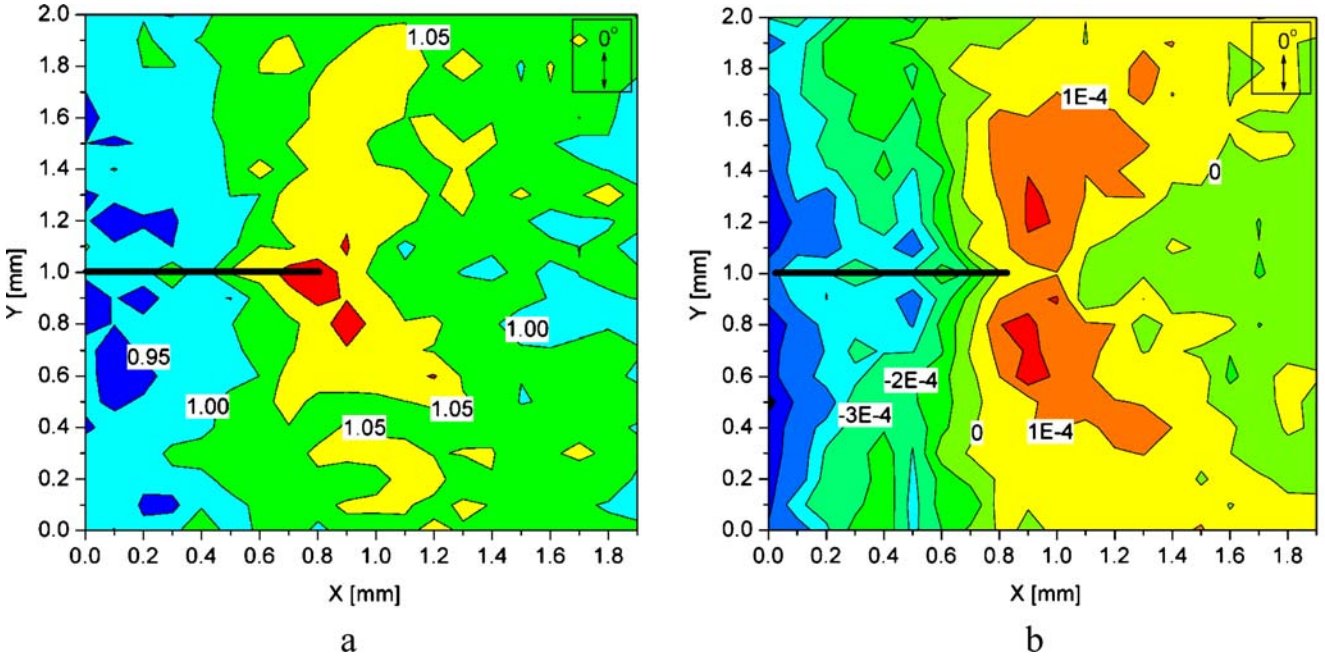

Fig. 8 Degree of domain switching (**a**) and 111 lattice strain (**b**) perpendicular to a crack tip loaded with a stress intensity factor just below the initiation toughness. Crack face is identified using a *bold line* at Y=1.0 mm. Measurements were taken in the crack front and wake of a tetragonal PZT ceramic measured using a microdiffraction approach. In (**a**), the relative presence of the 002 axis perpendicular to the crack face is described using a multiple of a random distribution (*mrd*) [Jones and Üstündag, unpublished work]

performance and reliability of a wide variety of piezoelectric devices are a function of this dynamic behavior.

9 Time-resolved techniques

As mentioned in the previous section, real-time diffraction measurements are possible with high-flux sources. Such measurements are very valuable in the characterization of piezoelectric materials because their electromechanical response can be time-dependent. For example, Grigoriev et al. have demonstrated that motion of a 180° ferroelectric domain wall in a tetragonal PZT thin film could be mapped both spatially and temporally using time-resolved microdiffraction [93]. They found a 180° domain wall to move at a velocity of 40 m/s.

Lower flux sources such as laboratory X-rays and neutrons can also be used in the characterization of longer time-scale processes. For example, the reaction kinetics in the processing of piezoelectric materials has been studied by Misture [46]. These measurements are enabled using a linear position sensitive detector with a laboratory X-ray source. When the process under investigation is repeatable, lower flux sources such as laboratory X-rays and neutrons can also be utilized to characterize short time-scale processes by employing a stroboscopic data collection mode. A stroboscopic collection mode is where one high-frequency cycle is described by summing the time-resolved intensities collected during multiple cycles. This is accomplished by synchronizing either the incident intensity bursts or the collected diffracted intensity with the applied cyclic electric field [121, 122]. Using this approach to measure the shift in the (200) diffraction peak position in $BaTiO_3$ thin films, Zolotoyabko et al. reported the time-scale of the ferroelectric/ferroelastic response on the order of 10 ns [121]. Harrison et al. employed stroboscopic data collection later to characterize the stress-induced ferroelastic response in $LaAlO_3$ single crystals [123].

Recently, Jones et al. have used stroboscopic methods to measure non-180° ferroelectric domain switching during sub-coercive electric field cycling in a bulk, tetragonal PZT ceramic. Using electric fields of 1 Hz and amplitude of half of the coercive field, they found a small yet measurable degree of domain switching [92, 124]. The time-resolved response of the 002_{pc} peaks to a bipolar square wave of half of the coercive field is shown in Fig. 9. Taking these measurements at multiple orientations relative to the electric field, they characterized all possible domain wall orientations, enabling a quantitative assessment of the degree to which non-180° domain switching contributes to the macroscopic strain. Using unipolar driving fields, they determined that the apparent bulk piezoelectric coefficient of 400 pm/V is comprised of ~34% which results from non-180° domain switching.

Given the dynamic nature of certain piezoelectric applications and the time- and frequency-dependence of many ferroelectric/ferroelastic properties, there are more opportunities for continued research utilizing time-resolved

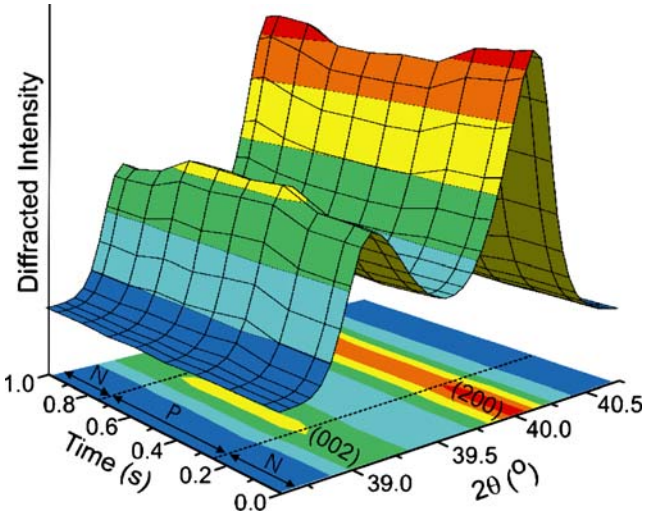

Fig. 9 Diffracted intensities of the pseudo-cubic 002 reflections as a function of 2θ and time during application of a square, bipolar electric field waveform of frequency 1 Hz and amplitude $\pm 0.5 \times E_c$. The time-scale is described using eight steps. The positive (*P*) state of the electric field is applied between 0.25 and 0.75 s, which is bounded on either side by the negative (*N*) field state. Diffracting vectors 002 and 200 are parallel to the applied electric field (reprinted with permission from Jones et al. [92], Copyright 2006, American Institute of Physics)

techniques. For example, the techniques already presented can be used to characterize differences in domain wall velocity as a function of defect and dopant concentration or grain orientation. The study of interphase boundary motion and its contribution to the electric-field-induced strain should also be explored using diffraction. There are also opportunities for applying these methods to more completely characterize the evolution of piezoelectric materials including creep [125] and ferroelastic switching fatigue [126, 127].

10 Future opportunities

X-ray and neutron diffraction are certain to provide continued opportunities in characterizing piezoelectric materials. Each section above posed individual opportunities for the continued use of diffraction in solving problems within this field. This section is devoted to eliciting some opportunities for combining the above techniques. Such combinatorial approaches take advantage of the increasing dimensionality of the characterization capabilities being developed within each topical area.

The applications of time-resolved approaches in the characterization of domain structures are just beginning to be realized. In addition to the wealth of information that can be gained regarding domain structures, the time-dependent measurement of diffuse scattering or superlattice reflections can enable the study of defects and structural ordering as a function of time. The combination of structure determination (whether crystal structure or short-range ordering) with micro-diffraction techniques can enable spatial heterogeneity of the structure to be characterized. This approach is particularly valuable in determining the influence of macroscopic geometric features such as cracks, electrode edges, and other interfaces and crystal defects such as domain walls.

Though the calculated value of spontaneous polarization from a structure refinement should be interpreted with caution, there is value in coupling this calculation to an orientation distribution function which represents ferroelastic or ferroelectric switching. This opportunity was mentioned previously in Section 5. A more accurate approach to such a relationship, however, might employ an anisotropic structure refinement during electrical loading (Section 2). Thus, crystals oriented at varying directions to the electric field exhibit different values of spontaneous polarization. For the case of ferroelastic switching, the contribution of non-180° domain switching to the developed bulk polarization can be extracted. If polarization inversion is measured as demonstrated by Grigoriev et al. [93], the contribution of 180° switching can also be extracted. If further investigated using time-resolved techniques (Section 9), such characterization approaches could describe completely the extrinsic contributions to the piezoelectric effect in ferroelectric ceramics. It would also be valuable to use such measurements in the validation of theoretical models of such behavior, which have started to be developed [128].

Other valuable opportunities exist in the coupling of diffraction with theoretical models. Such approaches help validate models so they can be used predictively. Li et al. have recently presented such a coupled experimental and theoretical approach to describe the switching behavior near the MPB in PZT ceramics [129]. Comparing their strain compatibility calculations to neutron diffraction measurements, they find that polycrystalline PZT ceramics consisting of both a rhombohedral and tetragonal phase can switch more easily than ceramics consisting of only one of these phases. Similarly, though both domain switching distributions have been measured [85, 91] and constitutive models exist that predict domain switching (e.g., [130, 131]), there have been no thorough comparisons between these approaches.

11 Concluding remarks

The use of diffraction in the characterization of piezoelectric materials has evolved in recent years. While many opportunities still exist in characterizing structure, phases, strains, and texture, new opportunities are rapidly evolving in the areas of microdiffraction and time-resolved techniques. These new characterization approaches offer the opportunity

to understand more completely the piezoelectric effect in bulk polycrystalline ceramic materials. Both the use of combinatorial characterization techniques and the coupling of diffraction measurements to theoretical models will help solve many current problems within this field.

Acknowledgments The author acknowledges valuable discussions on this topic with Keith Bowman, John Daniels, Andrew Studer, and Ersan Üstündag. Support from the US National Science Foundation, Award no. OISE-0402066, is gratefully acknowledged.

References

1. E.C. Subbarao, M.C. McQuarrie, W.R. Buessem, J. Appl. Phys. **28**, 1194 (1957)
2. B.D. Cullity, *Elements of X-ray Diffraction*, 2nd ed. (Addison-Wesley, Reading, MA, USA, 1978), p. 335
3. B. Noheda, J.A. Gonzalo, L.E. Cross, R. Guo, S.-E. Park, D.E. Cox, G. Shirane, Phys. Rev. B **61**, 8687 (2000)
4. H.M. Rietveld, J. Appl. Crystallogr. **2**, 65 (1969)
5. L.B. McCuster, R.B. Von Dreele, D.E. Cox, D. Louer, P. Scardi, J. Appl. Crystallogr. **32**, 36 (1999)
6. R.A. Young, E. Prince, R.A. Sparks, J. Appl. Crystallogr. **15**, 357 (1982)
7. R.A. Young, *The Rietveld Method* (Oxford University Press, Oxford, UK, 1995)
8. A.K. Cheetham, in *Structure Determination from Powder Diffraction Data*, ed. by W.I.F. David, K. Shankland, L.B. McCusker, Ch. Baerlocher (International Union of Crystallography, 2002), p. 13
9. C. Bedoya, Ch. Muller, J.-L. Baudour, V. Madigou, M. Anne, M. Roubin, Mater. Sci. Eng. B **75**, 43 (2000)
10. D.L. Corker, A.M. Glazer, R.W. Whatmore, A. Stallard, F. Fauth, J. Phys: Condens. Matter **10**, 6251 (1998)
11. J. Rouquette, J. Haines, V. Bornand, M. Pintard, Ph. Papet, W.G. Marshall, S. Hull, Phys. Rev. B **71**, 024112 (2005)
12. J.S. Forrester, E.H. Kisi, K.S. Knight, C.J. Howard, J. Phys.: Condens. Matter **18**, L233 (2006)
13. A.K. Singh, D. Pandey, Phys. Rev. B **67**, 064102 (2003)
14. A.K. Singh, D. Pandey, O. Zaharko, Phys. Rev. B **68**, 172103 (2003)
15. A.K. Singh, D. Pandey, O. Zaharko, Phys. Rev. B **74**, 024101 (2006)
16. J.-M. Kiat, Y. Uesu, B. Dkhil, M. Matsuda, C. Malibert, G. Calvarin, Phys. Rev. B **65**, 064106 (2002)
17. R.M. Ibberson, S.M. Moussa, M.J. Rosseinsky, A.N. Fitch, D. Iddles, T. Price, J. Am. Ceram. Soc. **89**, 1827 (2006)
18. I. Masuda, K.-I. Kakimoto, H. Ohsato, J. Electroceramics **13**, 555 (2004)
19. J.L. Jones, E.B. Slamovich, K.J. Bowman, J. Mater. Res. **19**, 3414 (2004)
20. Ismunandar, T. Kamiyama, A. Hoshikawa, Q. Zhou, B.J. Kennedy, Y. Kubota, K. Kato, J. Solid State Chem., **177**, 4188 (2004)
21. A. Le Bail, H. Duroy, J.L. Fourquet, Mater. Res. Bull. **23**, 447 (1988)
22. A. Sani, B. Noheda, I.A. Kornev, L. Bellaiche, P. Bouvier, J. Kreisel, Phys. Rev. B **69**, 020105(R) (2004)
23. Y. Shimakawa, Y. Kubo, Y. Nakagawa, T. Kamiyama, H. Asano, F. Izumi, Appl. Phys. Lett., **74**, 1904 (1999)
24. R.B. Von Dreele, in *The Rietveld Method*, ed. by R.A. Young (International Union of Crystallography, 1993), p. 227
25. N.C. Popa, D. Balzar, J. Appl. Crystallogr. **34**, 187 (2001)
26. J.V. Bernier, M.P. Miller, J. Appl. Crystallogr. **39**, 358 (2006)
27. S.J.L. Billinge, M.G. Kanatzidis, Chem. Comm. 749 (2004)
28. P. Juhás, D.M. Cherba, P.M. Duxbury, W.F. Punch, S.J.L. Billinge, Nature **440**, 655 (2006)
29. A. Sehirlioglu, D.A. Payne, S.R. Wilson, P. Han, Appl. Phys. Lett. **89**, 092903 (2006)
30. Y.M. Jin, Y.U. Wang, A.G. Khachaturyan, J.F. Li, D. Viehland, Phys. Rev. Lett. **91**, 197601 (2003)
31. Y.M. Jin, Y.U. Wang, A.G. Khachaturyan, J.F. Li, D. Viehland, J. Appl. Phys **94**, 3629 (2003)
32. F. Bai, J. Li, D. Viehland, J. Appl. Phys. **97**, 054103 (2005)
33. H. He, X. Tan, Phys. Rev. B. **72**, 024102 (2005)
34. W. Dmowski, T. Egami, L. Farber, P. K. Davies, in *Fundamental Physics of Ferroelectrics 2001*, ed. by H. Krakauer (American Institute of Physics, 2001), p. 33
35. T. Egami, W. Dmowski, Ceram. Trans. **136**, 3 (2003)
36. N.C. Popa, J. Appl. Crystallogr., **25**, 611 (1992)
37. S. Matthies, L. Lutterotti, H.R. Wenk, J. Appl. Crystallogr. **30** 31 (1997)
38. D.C. Lupascu, M. Hammer, Phys. Status Solidi. A **191**, 643 (2002)
39. D. Damjanovic, J. Am. Ceram. Soc. **88**, 2663 (2005)
40. B. Noheda, D.E. Cox, G. Shirane, J.A. Gonzalo, L.E. Cross, S.-E. Park, Appl. Phys. Lett. **74**, 2059 (1999)
41. R. Guo, L.E. Cross, S.-E. Park, B. Noheda, D.E. Cox, G. Shirane, Phys. Rev. Lett. **84**, 5423 (2000)
42. B. Noheda, D.E. Cox, Phase Transit. **79**, 5 (2006)
43. M. Davis, *J. Electroceramics* (in press)
44. M.J. Hoffmann, M. Hammer, A. Endriss, D.C Lupascu, Acta Mater. **49**, 1301 (2001)
45. R.C. Rogan, E. Üstündag, B. Clausen, M.R. Daymond, J. Appl. Phys. **93**, 4104 (2003)
46. S.T. Misture, J. Electroceramics **16**, 167 (2006)
47. U.F. Kocks, C.N. Tomé, H.-R. Wenk, *Texture and Anisotropy* (Cambridge University Press, Cambridge, UK, 2000)
48. J.L. Jones, E.B. Slamovich, K.J. Bowman, Mater. Sci. Forum **495–497**, 1401 (2005)
49. T. Takenaka, K. Sakata, J. Appl. Phys. **55**, 1092 (1984)
50. B.H. Venkataraman, K.B.R. Varma, J. Mater. Sci. **38**, 4895 (2003)
51. Y. Sakuma, T. Kimura, J. Electroceramics **13**, 537 (2004)
52. J.L. Jones, E.B. Slamovich, K.J. Bowman, D.C. Lupascu, J. Appl. Phys. **98**, 104102 (2005)
53. M.V. Gelfuso, D. Thomazini, J.A. Eiras, J. Am. Ceram. Soc. **82**, 2368 (1999)
54. J.S. Patwardhan, M.N. Rahaman, J. Mater. Sci. **39**, 133 (2004)
55. C. Duran, S. Trolier-McKinstry, G.L. Messing, J. Mater. Res. **18**, 228 (2003)
56. W. Chen, Y. Kinemuchi, K. Watari, T. Tamura, K. Miwa, J. Am. Ceram. Soc. **89**, 381 (2006)
57. E.M. Sabolsky, A.R. James, S. Kwon, S. Trolier-McKinstry, G. L. Messing, Appl. Phys. Lett. **78**, 2551 (2001)
58. S. Kwon, E.M. Sabolsky, G.L. Messing, S. Trolier-McKinstry, J. Am. Ceram. Soc. **88**, 312 (2005)
59. K.H. Brosnan, G.L. Messing, R.J. Meyer Jr., M.D. Vaudin, J. Am. Ceram. Soc. **89**, 1965 (2006)
60. H. Yilmaz, G.L. Messing, S. Trolier-McKinstry, J. Electroceramics **11**, 207 (2003)
61. H. Yilmaz, S. Trolier-McKinstry, G.L. Messing, J. Electroceramics **11**, 217 (2003)
62. G.L. Messing, S. Trolier-McKinstry, E.M. Sabolsky, C. Duran, S. Kwon, B. Brahmaroutu, P. Park, H. Yilmaz, P.W. Rehrig, K.B. Eitel, E. Suvaci, M. Seabaugh, K.S. Oh, Crit. Rev. Solid State Mater. Sci. **29**, 45 (2004)
63. F.K. Lotgering, J. Inorg. Nucl. Chem. **9**, 113 (1959)

64. A. March, Z. Kristallogr. Mineral. Petrogr./Abteilung A. **81**, 285 (1932)
65. W.A. Dollase, J. Appl. Crystallogr. **19**, 267 (1986)
66. H.-J. Bunge, *Texture Analysis in Materials Science* (Butterworths, London, UK, 1982)
67. H.-R. Wenk, *Preferred Orientation in Deformed Metals and Rocks: An Introduction to Modern Texture Analysis* (Academic, Orlando, FL, USA, 1985).
68. H.-R. Wenk, L. Lutterotti, S.C. Vogel, Nucl. Instr. Meth. Phys. Res. A, **515**, 575 (2003)
69. J.L. Jones, S.C. Vogel, E.B. Slamovich, K.J. Bowman, Scripta Mater. **51**, 1123 (2004)
70. J. Ricote, D. Chateigner, L. Pardo, M. Algueró, J. Mendiola, M. L. Calzada, Ferroelectrics **241**, 167 (2000)
71. J. Ricote, D. Chateigner, Ceramic Y Vidrio **38**, 587 (1999)
72. J. Ricote, D. Chateigner, J. Appl. Crystallogr. **37**, 91 (2004)
73. R.E. Garcia, W.C. Carter, S.A. Langer, J. Am. Ceram. Soc. **88**, 750 (2005)
74. J.A. Ruglovsky, J. Li, K. Bhattacharya, H.A. Atwater, Acta Mater. **54**, 3657 (2006)
75. H.J. Bunge, R.A. Schwarzer, Adv. Eng. Mater. **3**, 25 (2001)
76. K.J. Bowman, I.-W. Chen, J. Am. Ceram. Soc. **76**, 113 (1993)
77. M.G. Cain, S.M. Bennington, M.H. Lewis, S. Hull, Phil. Mag. B **69**, 499 (1994)
78. Y. Ma, E.H. Kisi, S.J. Kennedy, A.J. Studer, J. Am. Ceram. Soc. **87**, 465 (2004)
79. K. Kleveland, N. Orlovskaya, T. Grande, A. M.M. Moe, M.-A. Einarsrud, K. Breder, Gogotsi, J. Am. Ceram. Soc. **84**, 2029 (2001)
80. S. Faaland, T. Grande, M.-A. Einarsrud, P.E. Vullum, R. Holmestad, J. Am. Ceram. Soc. **88**, 726 (2005)
81. P.E. Vullum, J. Mastin, J. Wright, M.-A. Einarsrud, R. Holmestad, T. Grande, Acta Mater., **54**, 2615 (2006)
82. J.L. Jones, M. Hoffman, K.J. Bowman, J. Appl. Phys. **98**, 024115 (2005)
83. J.S. Forrester, E.H. Kisi, A.J. Studer, J. Eur. Ceram. Soc. **25**, 447 (2005)
84. D.A. Hall, A. Steuwer, B. Cherdhirunkorn, T. Mori, P.J. Withers, Acta Mater. **54**, 3075 (2006)
85. J.L. Jones, E.B. Slamovich, K.J. Bowman, J. Appl. Phys. **97**, 034113 (2005)
86. S. Hackemann, W. Pfeiffer, J. Eur. Ceram. Soc. **23**, 1414 (2003)
87. D.A. Hall, A. Steuwer, B. Cherdhirunkorn, P.J. Withers, T. Mori, Mater. Sci. Eng. A **409**, 206 (2005)
88. X. Zheng, J. Li, Y. Zhou, Acta Mater. **52**, 3313 (2004)
89. W. Chang, A. King, K.J. Bowman, Appl. Phys. Lett. **88**, 242901 (2006)
90. J.E. Daniels, J.L. Jones, T.R. Finlayson, J. Phys. D: Appl Phys **39**, 5294 (2006)
91. J.L. Jones, M. Hoffman, S.C. Vogel, Mech. Mater. **39**, 283 (2007)
92. J.L. Jones, M. Hoffman, J.E. Daniels, A.J. Studer, Appl. Phys. Lett. **89**, 092901 (2006)
93. A. Grigoriev, D.-H. Do, D.M. Kim, C.-B. Eom, B. Adams, E.M. Dufresne, P.G. Evans, Phys. Rev. Lett. **96**, 187601 (2006)
94. Q. Du, J. Li, W. Nothwang, M.W. Cole, Acta Mater., **54**, 2577 (2006)
95. A. Sehirlioglu, D.A. Payne, P. Han, Phys. Rev. B, **72**, 214110 (2005)
96. K.R. Kendall, C. Navas, J.K. Thomas, H.-C. zur Loye, Chem. Mater. **8**, 642 (1996)
97. R.R. Das, D.M. Kim, S.H. Baek, C.B. Eom, F. Zavaliche, S.Y. Yang, R. Ramesh, Y.B. Chen, X.Q. Pan, X. Ke, M.S. Rzchowski, S.K. Streiffer, Appl. Phys. Lett. **88**, 242904 (2006)
98. B.D. Cullity, *Elements of X-ray Diffraction*, 2nd ed. (Addison-Wesley, Reading, MA, USA, 1978), p. 447
99. A. Endriss, M. Hammer, M.J. Hoffmann, A. Kolleck, G.A. Schneider, J. Eur. Ceram. Soc. **19**, 1229 (1999)
100. J.-T. Reszat, A.E. Glazounov, M.J. Hoffmann, J. Eur. Ceram. Soc. **21**, 1249 (2001)
101. D.A. Hall, A. Steuwer, B. Cherdhirunkorn, T. Mori, P.J. Withers, J. Appl. Phys. **96**, 4245 (2004)
102. X.-h. Du, J. Zheng, U. Belegundu, K. Uchino, Appl. Phys. Lett. **72**, 2421 (1998)
103. M. Budimir, D. Damjanovic, N. Setter, Phys. Rev. B, **73**, 174106 (2006)
104. A.J. Bell, J. Mater. Sci. **41**, 13 (2006)
105. D. Damjanovic, M. Budimir, M. Davis, N. Setter, J. Mater. Sci. **41**, 65 (2006)
106. J.L. Jones, M. Hoffman, J. Am. Ceram. Soc. **89**, 3721 (2006)
107. K. Shirakihara, K. Tanaka, Y. Akiniwa, Y. Sakaida, H. Mukai, Mater. Sci. Res. Intl. **8**, 26 (2002)
108. J.L. Jones, M. Hoffman, S.C. Vogel, Physica B **385–386**, 548 (2006)
109. M.R. Daymond, M.A.M. Bourke, R.B. Von Dreele, B. Clausen, T. Lorentzen, J. Appl. Phys. **82**, 1554 (1997)
110. M.R. Daymond, J. Appl. Phys. **96**, 4263 (2004)
111. A.I. Ustinov, J.-C. Niepce, C. Valot, L.A. Olikhovska, F. Bernard, Mater. Sci. Forum **321–324**, 109 (2000)
112. S.A. Hayward, E.K.H. Salje, Z. Kristallogr. **220**, 994 (2005)
113. H. Boysen, Z. Kristallogr. **220**, 726 (2005)
114. A.M. Glazer, P.A. Thomas, K.Z. Baba-Kishi, G.K.H. Pang, C.W. Tai, Phys. Rev. B. **70**, 184123 (2004)
115. C. Stock, D. Ellis, I.P. Swainson, G. Xu, H. Hiraka, Z. Zhong, H. Luo, X. Zhao, D. Viehland, R.J. Birgeneau, G. Shirane, Phys. Rev. B **73**, 064107 (2006)
116. G. Xu, Z. Zhong, Y. Bing, Z.-G. Ye, G. Shirane, Nature Mater. **5**, 134 (2006)
117. R.C. Rogan, N. Tamura, G.A. Swift, E. Üstündag, Nature Mater. **2**, 379 (2003)
118. D.-H. Do, P.G. Evans, E.D. Isaacs, D.M. Kim, C.B. Eom, E.M. Dufresne, Nature Mater. **3**, 365 (2004)
119. B. Jakobsen, H.F. Poulsen, U. Lienert, J. Almer, S.D. Shastri, H.O. Sørensen, C. Gundlach, W. Pantleon, Science **312**, 889 (2006)
120. D. Juul Jensen, E.M. Lauridsen, L. Margulies, H.F. Poulsen, S. Schmidt, H. O. Sørensen, G.B.M. Vaughan, Materials Today **9**, 18 (2006)
121. E. Zolotoyabko, J.P. Quintana, B.H. Hoerman, B.W. Wessels, Appl. Phys. Lett. **80**, 3159 (2002)
122. G. Eckold, H. Gibhardt, D. Caspary, P Elter, K. Elisbihani, Z. Kristallogr. **218**, 144 (2003)
123. R.J. Harrison, S.A. T. Redfern, A. Buckley, E.K. H. Salje, J. Appl. Phys. **95**, 1706 (2004)
124. J.L. Jones, M. Hoffman, J.E. Daniels, A.J. Studer, Physica B **385–386**, 100 (2006)
125. Q.D. Liu, J.E. Huber, J. Eur. Ceram. Soc. **26**, 2799 (2006)
126. J.L. Jones, C.R.J. Salz, M. Hoffman, J. Am. Ceram. Soc., **88**, 2788 (2005)
127. D.C. Lupascu, J. Rödel, Adv. Eng. Mater. **7**, 882 (2005)
128. S. Trolier-McKinstry, N.B. Gharb, D. Damjanovic, Appl. Phys. Lett. **88**, 202901 (2006)
129. J.Y. Li, R.C. Rogan, E. Üstündag, K. Bhattacharya, Nature Mater. **4**, 776 (2005)
130. C.M. Landis, Current Opin. Solid State Mater. Sci. **8**, 59 (2004)
131. J.E. Huber, Current Opin. Solid State Mater. Sci. **9**, 100 (2005)